Molecular Crystals and Liquid Crystals

ISSN: 1542-1406 (Print) 1563-5287 (Online) Journal homepage: http://www.tandfonline.com/loi/gmcl20

Origin of Hopping Dynamics in Hexatic Smectic B and Smectic A Liquid Crystals

Keiko M. Aoki

To cite this article: Keiko M. Aoki (2015) Origin of Hopping Dynamics in Hexatic Smectic B and Smectic A Liquid Crystals, Molecular Crystals and Liquid Crystals, 612:1, 72-80, DOI: 10.1080/15421406.2015.1030576

To link to this article: http://dx.doi.org/10.1080/15421406.2015.1030576

Published online: 06 Jul 2015.

Mol. Cryst. Liq. Cryst., Vol. 612: pp. 72–80, 2015
Published with license by Taylor & Francis Group
ISSN: 1542-1406 print/1563-5287 online
DOI: 10.1080/15421406.2015.1030576

Origin of Hopping Dynamics in Hexatic Smectic B and Smectic A Liquid Crystals

KEIKO M. AOKI[1,2,3,*]

[1]iCFD, Meguro-ku, Tokyo, Japan
[2]Faculty of Science, Toho University, Funabashi, Japan
[3]Faculty of Science and Engineering, Waseda University, Tokyo, Japan

Origin of hopping dynamics in liquid crystals is investigated by constant-pressure and constant-temperature molecular dynamics simulations. Hopping dynamics is observed in both hexatic smectic B (HexB) and smectic A (SmA) liquid crystals, however in different directions. At the crystal-Hex B transition, a second order transtition occurs where the layer thickness increases continuously. At the HexB-SmA transition, melting inside the layers is observed. The hopping occurs in the direction normal to the direction with loose density, i.e., *xy-direction in HexB and z-direction in SmA.*

Keywords liquid crystals; smectic A; hexatic smectic B; molecular dynamics simulation; hopping dynamics

1. Introduction

The solutions of symplectic integrators preserve the structure of the Hamilton's equations of motion. Recent molecular dynamics simulations using the symplectic integrator designed for soft matter [1] has shown the nature of crystal-hexatic smectic B(HexB)-smectic A(SmA) phase transition [2, 3]. Hopping dynamics occur in both HexB and SmA liquid crystals (LC's). The hopping in SmA phase occurs among the smectic layers (one-dimensionally), while hopping in HexB phase occurs inside the layers (two-dimensionally). The dynamical aspect of both phases has been reported in [4]. The temperature dependence of diffusion coefficients of hopping in SmA phase can be described by the Arrhenius equation characteristic of activation process. In HexB LC phase, the diffusion coefficients saturate at higher temperatures. Hopping dynamics in glass has been known for quite a long time but the origin is still not quite clear. In this paper, the origin of the hopping dynamics in LC is investigated in relation to the anisotropy of the packing of the molecules.

*Address correspondence to Keiko M. Aoki, iCFD, 1-16-5 Haramachi, Meguro-ku, Tokyo 152-0011, Japan; E-mail: aoki@icfd.co.jp

Color versions of one or more of the figures in the article can be found online at www.tandfonline.com/gmcl.

2. Simulation Model and Method

2.1. Model

The model particles are parallel soft spherocylinders [2, 3] interacting through purely repulsive pairwise potential expressed by minimum distance between the particles;

$$\phi_{ij} = \begin{cases} \varepsilon \left[\left(\dfrac{d}{R_{ij}} \right)^{12} - \left(\dfrac{d}{R_{ij}} \right)^{6} + \dfrac{1}{4} \right] & \text{if} \quad R_{ij} < r_0 \\ 0 & \text{otherwise,} \end{cases} \tag{1}$$

where $r_0 = 2^{1/6} d$ and R_{ij} is the shortest distance between lines representing the long axis of two spherocylinders i and j:

$$R_{ij}^2 = \begin{cases} x_{ij}^2 + y_{ij}^2 & \text{if } |z_{ij}| \leq L \\ x_{ij}^2 + y_{ij}^2 + \left(|z_{ij}| - L \right)^2 & \text{otherwise,} \end{cases} \tag{2}$$

where (x_{ij}, y_{ij}, z_{ij}) is the relative position of the center of mass the spherocylinders i and j, and L is the length of the line representing the long axis of the spherocylinder which is fixed parallel to the z-axis. Stable HexB phase do not appear in systems of purely repulsive spherocylinders with rotation, at least for moderate anisotropy, i.e., $L \leq 5$ [5]. By hindering the rotation of the long axis, the HexB phase becomes a thermodynamic equilibrium phase consistent with the fact that the orientational order of the long axis is generally very high in HexB phase. Periodic boundary conditions are applied in x, y, and z-directions. Reduced units where length, energy, and mass are measured in D, ε, m (where m is the mass of a spherocylinder), respectively, are used throughout this work.

2.2. Symplectic integrator designed for soft matter

Recently the present author developed an explicit symplectic integrator [1] for soft matter simulation. In this method, the pressure is treated as a tensor to ensure the system to be under hydrostatic pressure [6]. In liquid crystal phases, the shape of the molecular volume changes with temperature, thus it is important to use a flexible simulation cell for stress free simulations. On the other hand, there is a difference in the time scale of fluctuation depending on directions, *i.e,* layer undulation *vs.* intra-layer fluctuation. The large time scale differences require a simulation cell with rigidity to support the slow and large fluctuations. The barostat is designed to fulfill the above requirements. All the data reported in this work was obtained by constant hydrostatic pressure and constant temperature molecular dynamics simulations.

3. Results

3.1. Overview of crystal-HexB-SmA phase transition

The phase diagram of crystal-HexB-SmA phase transition for different molecular length L is given in [2].The crystal-HexB phase transition is 2nd order while the HexB-SmA phase transition is 1st order. To understand the nature of the phase sequence of crystal-HexB-SmA, the average intermolecular distance and layer thickness are shown in Figs. 1(a) and (b), respectively. Different colours denote systems with different core length L of the spherocylinder. They show that L_{xy} is discontinuous and L_z is continuous at the HexB-SmA transition, showing a feature of 2 dimensional melting. Both L_{xy} and L_z continuously

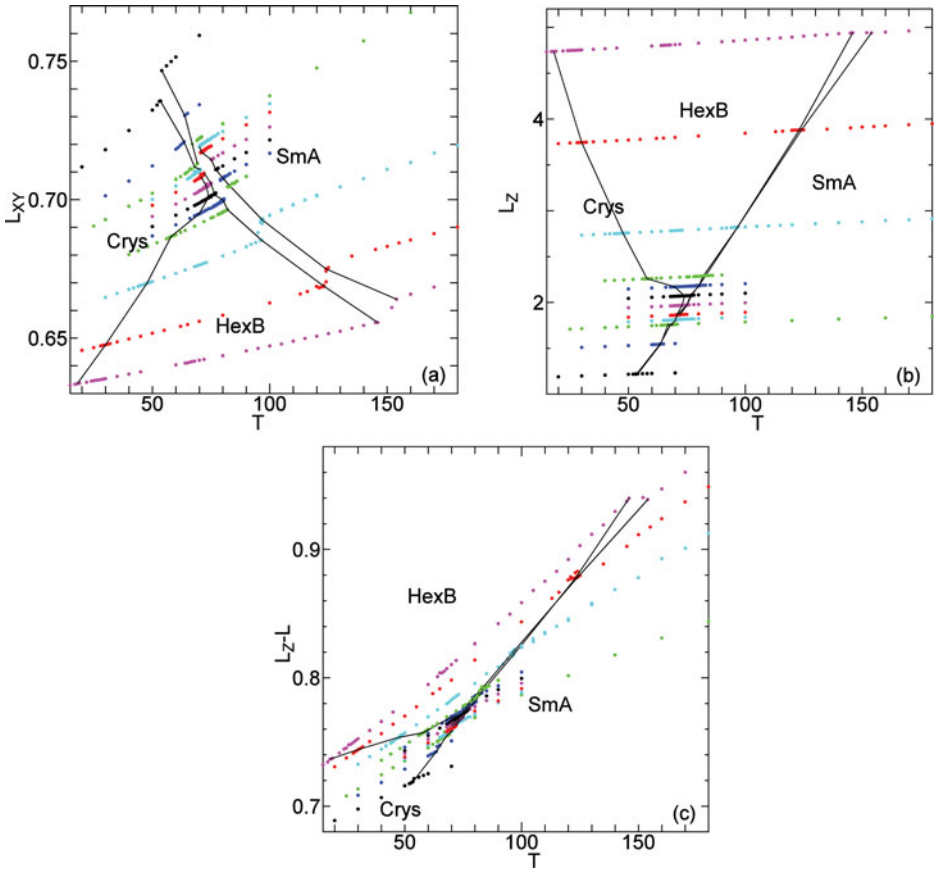

Figure 1. Average values of (a) intermolecular distance *Lxy* (b) layer thickness *Lz*, and (c) interlayer distance (*Lz*-*L*) for systems of soft parallel spherocylinders. Different colors denote different length. From the top of (a), and the bottom of (b) and (c), $L = 0.5$:●, $L = 0.8$:●, $L = 1.0$:●, $L = 1.05$:●, $L = 1.1$:●, $L = 1.2$:●, $L = 1.3$:●, $L = 1.4$:●, $L = 1.5$:●, $L = 2$:●, $L = 3$:●, $L = 4$:●.

increase at the crystal-HexB phase transition. Comparing the relative position of HexB and SmA phases in Fig. 1(a), it is understood that L_{xy} have larger values in SmA compared to HexB. The layer thickness L_z increase linearly against temperature as shown in Fig. 1(b). In Fig. 1(c), the interlayer distance (L_z-L) is plotted against the temperature. Subtracting the length of the core of the spherocylinder L by the layer thickness shows that the HexB phase have longer interlayer distance than the SmA phase for the same temperature (which is a comparison made between systems with different molecular length by nature). It can be said that it is relatively loose inside the layers in SmA and relatively loose between the layers in HexB.

3.2. HexB metastable states

A scaling relation of 6-fold bond orientational order (BOO) parameter and its higher harmonics have been reported by X-ray and netron scattering experiments [7]. Scaling relations in HexB phase has been observed in MD simulations [3] which also show that

there exist multiple metastable states of HexB liquid crystals. By calculating the 6-fold BOO of each layer, it has been revealed that the correlation among the layers is strong when the system is in thermodynamic equilibrium HexB phase. Depending on the strength of the correlation among the layers, a variety of metastable HexB states appear. We have seen in the previous subsection that in the HexB phase, it is dense inside the layer but comparatively loose between the layers. In this subsection, the physical properties of metastable HexB states are analysed.

Here we discuss systems of molecular rigid core length $L = 4$ and $L = 1.5$. In the phase diagram of our model, $L = 4$ is the longest molecular system where both the Crys-HexB and HexB-SmA phase transitions can be clearly detected. For longer molecules, the 1st order HexB-SmA phase transition can be clearly detected and obey the scaling properties of melting (the effective diameter is defined as the distance where interparticle potential energy and the system's temperature is equal) as in [8] (Calculations upto $L = 20$ has been made). The Crys-HexB phase transition is $T_{CB} = 18.0$ for system of $L = 4$, already close to the low temperature limit $T = 10$ for reliable calculations for the current pressure $P = 1000$. Thus, for systems with longer molecules, it was not possible to get a stable crystal phase. The HexB phase appear for $L \geq 1.1$ but for a narrow temperature range ($70.7 < T < 72$ for $L = 1.1$). For system of $L = 1.5$, the temperature range of HexB phase become wide enough to clearly observe the temperature dependence of physical properties.

In Fig. 2, the physical properties of molecular core length $L = 4$ are shown. The sixfold BOO C_6 is plotted against the temperature in Fig. 2(a). At temperatures $150 < T < 154$ the value of C_6 is strongly fluctuating, thus the data are omitted from Fig. 2. Additional metastable states appear compared to Fig. 1(b) of [3]. There are metastable states, mostly a pair or a set of 3, which have energy barrier nearly equivalent to the thermal fluctuation where the system stays in the basin of a pair (or a set of 3). Even in such dual state (or triple state), the values of C_6 for each basin are discernible as discrete values. Such fluctuation pair are also observed in the network of free-energy landscape of HexB as vertices connected with thick edges [9]. The network was constructed by analyzing HexB states at $T = 135$, *i.e.,* relatively close to the HexB-SmA transition temperature. However we observe such connected basins at a wide temperature range. Symbols ▼ and × represent fluctuating states for the temperature range $65 \leq T \leq 120$ and $70 \leq T \leq 112$, respectively. Figures 2 (b) and (c) show the relation of twelvefold BOO C_{12} and eighteenfold BOO C_{18} against sixfold BOO C_6, respectively. In Figs. 2 (b) and (c), temperature dependence from low to high can be traced by following the curve of each symbol from the right top to the left bottom. Comparison of ○ and ■ in Fig. 2(a), (b), and (c) show that they are different states with C_{12} having completely different values but closely related values of C_6 and C_{18}. At a small temperature range $56 \leq T \leq 58$, ■ consists an independent metastable state (possess different value of C_6 and C_{18} values) with C_{12} values on the branch of ○. Two values of ◇ at $T = 112$ and $T = 116$ are different independent states with high values of C_{12} and C_{18} compared to the main branch of ◇ at $T \leq 125$ shown in Figs. 2(b) and (c). Similarly, two values of ∇ at $T = 115$ and $T = 120$ consists a different branch in Figs. 2(b) and (c). Data obtained from the same initial configuration are denoted by the same symbol, thus it is shown that ◇ and ∇ bifurcate from the main branch at high temperatures.

By investigating the sixfold BOO in each layer with the sign,

$$A_6^l = \left\langle \frac{1}{N_b'} \sum_j^{N_l} \sum_k \cos\left(6\theta_{kj}\right) \right\rangle \tag{3}$$

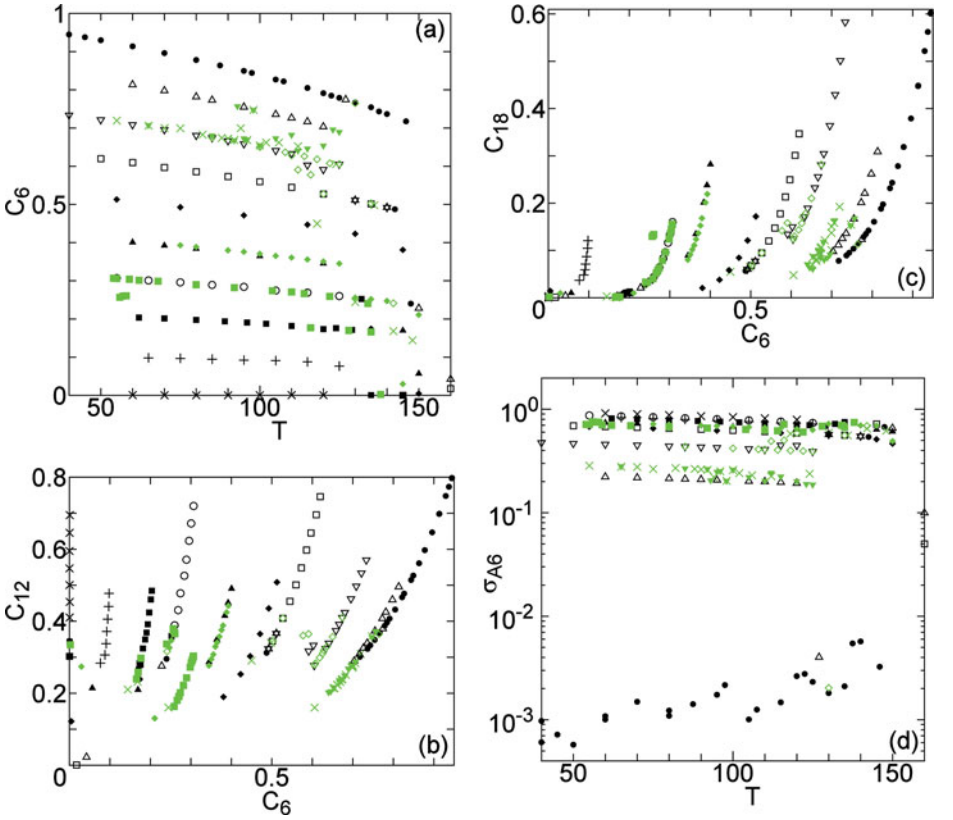

Figure 2. Temperature dependence of various properties of HexB metastable states and thermodynamic equilibrium HexB phase of system with core length $L = 4$ and $N = 1344$ which consists of 6 layers. The HexB-SmA transition occurs at $T = 154$. Data obtained from the same initial configuration (but are independent runs) are denoted by the same symbol. Symbols in green are data from a different initial configuration which are not reported in [3]. (a) Sixfold BOO versus temperature. (b) Twelvefold BOO versus sixfold BOO. (c) Eighteenfold BOO versus sixfold BOO. (d) Standard deviation σ_{A_6} of sixfold BOO with sign A_6 versus temperature.

the correlation among the layers is understood. Figure 2(d) shows the temperature dependence of the standard deviation of A_6, calculated as

$$\sigma_{A_6} = \sqrt{\frac{\sum_{l=1}^{n_l} \left(A_6^l\right)^2 - \left(\sum_{l=1}^{n_l} A_6^l\right)^2 / n_l}{n_l}} \tag{4}$$

where n_l is the number of layers. When σ_{A_6} is high the correlation among the layers is weak. Data with $\sigma_{A_6} < 10^{-2}$ corresponds to the thermodynamic equilibrium HexB phase. Metastable HexB states have various correlations with $\sigma_{A_6} > 10^{-1}$ and the SmA phase has values inbetween. The metastable HexB state with the largest value of σ_{A_6}(symobol $\times$), consists of layers with BOO differences of 30° on average (3 layers each), thus possess aniti-correlation among the layers. This explains why this state has $C_6 \simeq 0$, C_6 values smaller than in the SmA phase [see Fig. 2(a)]. Figure 2(d) also shows that states with close values of C_6 such as ($\circ$ and $\blacksquare$), or (∇ and $\times$) are different metastable states [as confirmed by

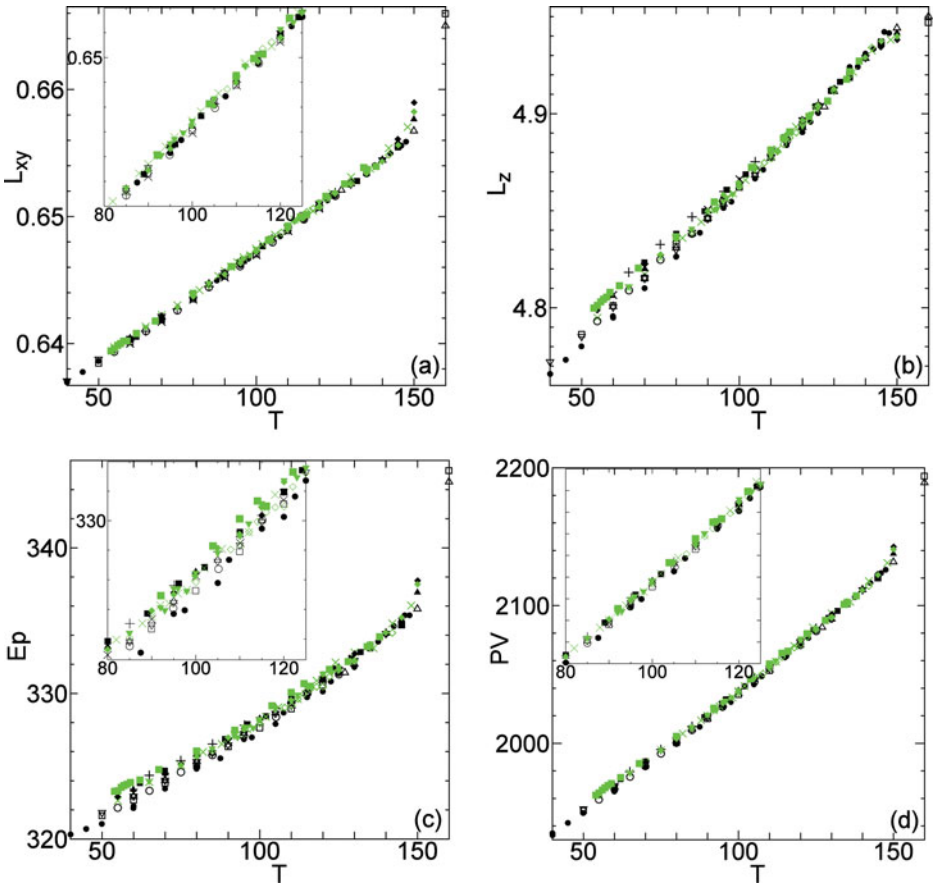

Figure 3. Temperature dependence of various properties of the same HexB metastable states and thermodynamic equilibrium HexB phase shown in Fig. 2. Average (a) intermolecular distance L_{xy}, (b) layer thickness L_z, (c) potential energy per molecule E_p, and (d) pressure multiplied by volume per molecule *PV*.

Figs. 2(b) and (c)]. Figures 3(a) and (b) show the temperature dependence of *Lxy* and *Lz*. Both values depend on the observed metastable state, however it is easier to detect a clear systematic dependence of each metastable state for *Lz*. In Fig. 3(c) and (d), the average potential energy and pressure multiplied by volume per molecule are shown. The average potential energy refects the packing of molecules thus the value of both *Lxy* and *Lz*.

In Figs. 4 and 5, we discuss systems of molecular rigid core length $L = 1.5$. Figure 4(a) shows temperature dependence of sixfold BOO C_6. For the same simulations, C_{12} and C_{18} along with other physical properties are calculated and shown in Figs. 4(b) through (d) and Fig. 5. In Figs. 4(b) and (c), following the curve of each symbols from the right top to the left bottom corresponds to data of temperature from low to high. It has been pointed out in the previous section for systems with $L = 4$, metastable states with close values C_6 of can be distinguished with C_{12}/C_{18}. Figures 4(a), (b), and (c) show that for the metastable states of $L = 1.5$, C_{12} and C_{18} also show close values when C_6 have close values for most of the case. However, (×, ●) and (△, ♦) clearly consists different branches in Figs. 4 (b) and 4(c). Note that ♦ at $T = 72$ and ● at $T = 76$ consists a different branch as shown in

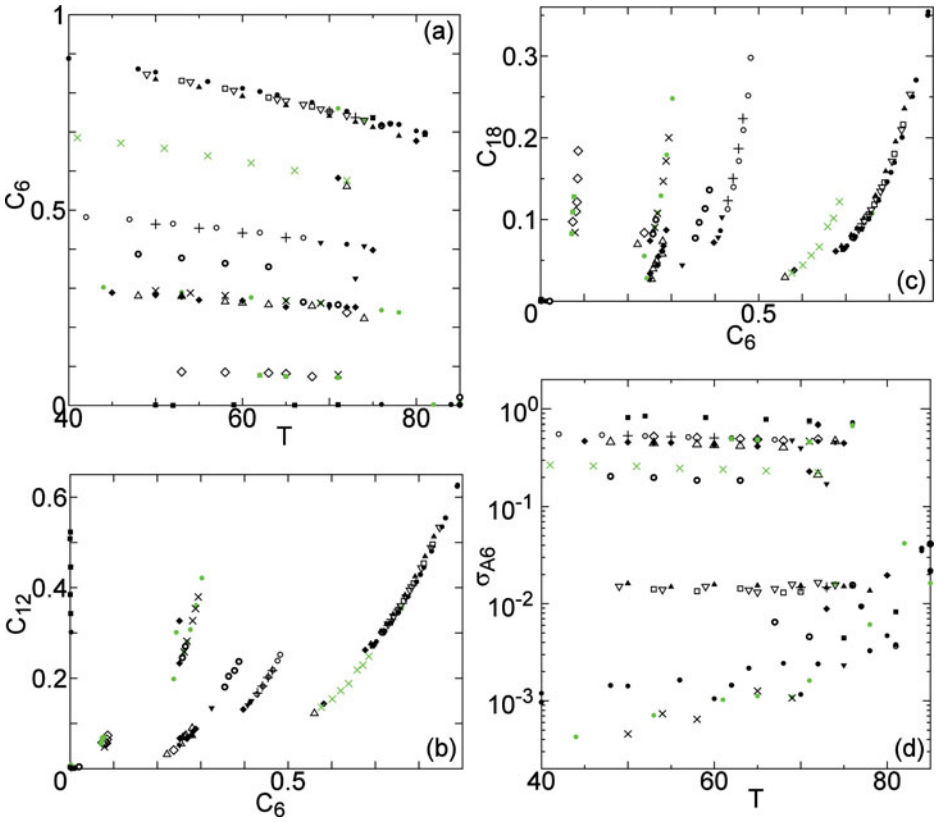

Figure 4. Temperature dependence of various properties of HexB metastable states and thermodynamic equilibrium HexB phase of system with core length $L = 1.5$ and $N = 1344$ which consists of 6 layers. The HexB-SmA transition occurs at $T = 83.4$. Data obtained from the same initial configuration (but are independent runs) are denoted by the same symbol. (a) Sixfold BOO versus temperature. (b) Twelvefold BOO versus sixfold BOO. (c) Eighteenfold BOO versus sixfold BOO. (d) Standard deviation σ_{A_6} of sixfold BOO with sign A_6 versus temperature.

Fig. 4 (b). Also note that $\diamond$ at $T = 72$ and $\triangle$ at $T = 74$ consists a different branch as shown in Fig. 4(c). The above two examples are bifurcation from the main branch of $C_6 \simeq 0.25$. Figure 4(d) shows σ_{A_6} for systems with molecular core length $L = 1.5$. The most strong correlation (lowest values of σ_{A_6}) are observed in metastable states denoted by $\times$ and $\bullet$. These states consists of 6 layers with similar values of C_6; Symbol $\times$ $C_6 = 0.30$ (at $T = 44$) to $C_6 = 0.26$ (at $T = 69$), and $\circ$ $C_6 = 0.29$ (at $T = 50$) to $C_6 = 0.26$ (at $T = 69$). The values of C_6 for systems denoted by ∇ , $\blacktriangle$, and $\square$ with σ_{A_6} in the order of 10^{-2} show high values of C_6 close to the thermodynamic equilibrium HexB phase denoted by $\bullet$ as shown in Fig. 4(a). However Fig. 4(d) clearly distinguish the metastable states from thermodynamic equilibrium HexB phase with σ_{A_6} at the order of 10^{-3}. As in the case of $L = 4$, the largest values of σ_{A_6} is for systems denoted by $\blacksquare$ with anti-correlation (30° difference in BOO) among layers, thus $C_6 \simeq 0$.

Figure 5 shows the temperature dependence of L_{xy}, L_z, E_p and PV for the same HexB states depicted in Fig. 4. In Fig. 5(b), the values of L_z is clearly divided in three branches.

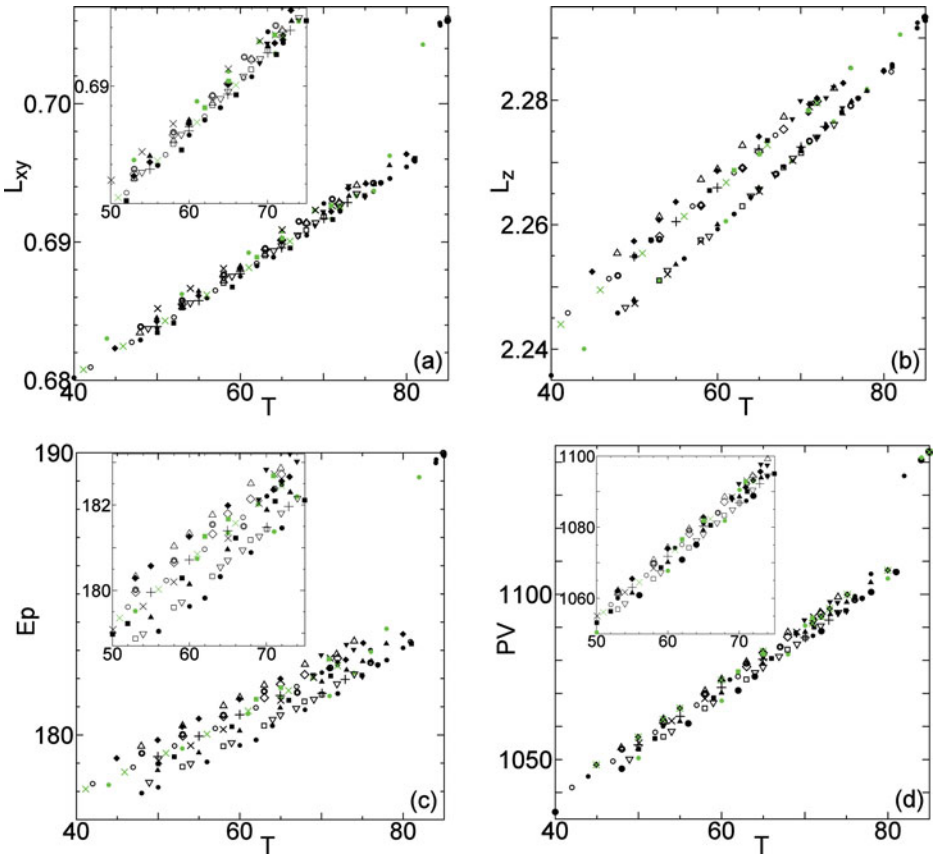

Figure 5. Temperature dependence of various properties of the same HexB metastable states and thermodynamic equilibrium HexB phase shown in Fig. 4. Temperature dependence of average (a) intermolecular distance L_{xy}, (b) layer thickness L_z, (c) potential energy per molecule E_p, and (d) pressure multiplied by volume per molecule PV.

3.3. SmA phase

The hopping dynamics in SmA phase for soft parallel spherocylinders show a clear linear dependence on time when observed for time $t > 10^3$ except for low temperatures near the HexB-SmA transition. The time scale where the non-Gaussian parameter $\alpha(t) \neq 0$ is much shorter compared to the hopping in HexB phase[4]. Mean square displacement becomes a linear function of time (where the inclination is the diffusion coefficient) when $\alpha(t) = 0$. When the temperature is high, the time scale to reach $\alpha(t) = 0$ becomes short. In the SmA phase, the temperature dependence of the diffusion coefficient D is described by the Arrhenius equation

$$D = D_0 \exp(-E/T) \tag{5}$$

in both directions parallel and perpendicular to the molecular axis as confirmed in experimental studies[10]. In SmA phase, the diffusion coefficient perpendicular to the molecular axis $D_\perp$ is $10^2 \sim 10^4$ times larger than that of the hopping diffusion parallel to the molecular axis $D_\parallel$ (see Fig. 2 of [4]). The activation energies and pre-exponential factors of diffusion

Table 1. Molecular length depeendence of activation energies $E_{\parallel}$, $E_{\perp}$ and pre-exponential factors $D_{\parallel 0}$, $D_{\perp 0}$ of diffusion parallel and perpendicular to the molecular axis and it's ratios in SmA phase

Length	$E_{\parallel}\,[\varepsilon]$	$D_{\parallel 0}\left[d\sqrt{\varepsilon/m}\right]$	$E_{\perp}\,[\varepsilon]$	$D_{\perp 0}\left[d\sqrt{\varepsilon/m}\right]$	$E_{\parallel}/E_{\perp}$	$D_{\parallel 0}/D_{\perp 0}$
2	1473	22.78	237.7	13.27	6.20	1.72
3	1913	27.47	322.9	15.20	5.92	1.81
4	2349	34.78	385.2	15.83	6.10	2.20

in SmA phase is shown in Table 1. The activation energy for hopping is one order larger than that of for the diffusion inside the layers.

4. Concluding Remarks

Systems of parallel soft spherocylinders with various molecular length are simulated. Hopping occurs in both the HexB and the SmA phase but in different directions. The temperature dependence of intra- and inter-molecular distance are different. It has been revealed that the interlayer distance in HexB phase is relatively large compared to that of SmA phase for the same temperature. Thus, HexB phase has a loose interlayer structure which lead to many different metastable HexB states with different BOO and layer correlation. In contrast to the melting to SmA phase where melting occur inside the layers, continuous increase of interlayer spacing occurs in direction normal to the layer at the crystal to HexB phase transition. Various physical properties are discussed for the metatstable HexB states. Activation energies are calculated for diffusion in SmA phase.

References

[1] Aoki, K. M. (2008), *J. Phys. Soc. Jpn.*, *77*, 044003; Aoki, K. M. (2014), *JPS Conf. Proc.*, *1*, 016009.
[2] Aoki, K. M., Yoneya, M., & Yokoyama, H. (2010), *Phys. Rev. E*, *81*, 021701.
[3] Aoki, K. M. & Yoneya, M. (2011), *J. Phys. Soc. Jpn.*, *80*, 124603.
[4] Aoki, K. M., Fujiwara, S., Sogo, K., Ohnishi, S., & Yamamoto, T.(2013), *Crystals*, *3*, 315; Aoki, K. M., Fujiwara, S., Sogo, K., Ohnishi, S., & Yamamoto, T. (2014), *JPS Conf. Proc.*, *1*, 012038.
[5] Aoki, K. M. & Akiyama, T. (1995), *Mol. Cryst. Liq. Cryst.*, *262*, 543; Aoki, K. M. & Akiyama, T. (1996), *Mol. Sim.*, *16*, 99; Aoki, K.M. & Akiyama, T. (1997), *Mol. Cryst. Liq. Cryst.*, *299*, 45; Al-Barwani, M. S. & Allen, M. P., (2000), *Phys. Rev. E*, *62*, 6706; Earl, D.J., Ilnytskyi, J., & Wilson, M. (2001), *Mol. Phys.*, *99*, 1719; Aoki, K. M., Yoneya, M., & Yokoyama, H. (2001), *Mol. Cryst. Liq. Cryst.*, *336*, 117; Aoki, K. M., Yoneya, M., & Yokoyama, H. (2003), *J. Chem. Phys.*, *118*, 9926; Aoki, K. M., Yoneya, M., & Yokoyama, H. (2004), *Mol. Cryst. Liq. Cryst.*, *413*, 109; Aoki, K. M., Yoneya, M., & Yokoyama, H. (2006), *J. Chem. Phys.*, *124*, 064705.
[6] Aoki, K. M., Yoneya, M., & Yokoyama, H. (2004), *J. Chem. Phys.*;*120*, 5576.
[7] Brock, J.D., Aharony, A., Birgeneau, R.J., Evans-Lutterodt, K.W., Lister, J.D., Horn, P.M., Stephenson, G.B., & Tajbakhsh, A.R. (1986), *Phys. Rev. Lett.*, *57*, 98; Chou, C-F., Ho, J.T., Hui, S.W., and Surendranath, V. (1996), *Phys. Rev. Lett.*, *76*, 4556.
[8] Aoki, K.M. and Yonezawa, F. (1993) *Phys. Rev. E*, *48*, 2025.
[9] Aoki, K. M. (2014). *J. Phys. Soc. Jpn.*, *83*, 104603.
[10] Krüger, G.J. (1982) *Phys. Rep.*, *82*, 229.